Available online at www.sciencedirect.com
SCIENCE DIRECT®
Catalysis Today 100 (2005) 3–9
CATALYSIS TODAY
www.elsevier.com/locate/cattod

Model studies on heterogeneous catalysts at the atomic level

Hans-Joachim Freund *

Fritz-Haber-Institut der Max-Planck-Gesellschaft, Department of Chemical Physics, Faradayweg 4-6, D-14195 Berlin, Germany

Available online 2 March 2005

Abstract

Model studies carried out on ultrahigh vacuum (UHV) prepared nanoparticles grown on well-ordered oxide surfaces allow insight into structure and reactivity of such systems at the atomic level. We review work on hydrogenation reactions of hydrocarbons on Pd metal particles addressing in particular the question of structure sensitivity and in a second example the preparation and characterization of supported vanadia monolayer catalysts for oxidation reactions. In the latter case we address the vibrational properties of vanadia ''monolayer model catalysts'' on alumina and on silica.

Keywords: Heterogeneous catalysts; Vanadia monolayer; Nanoparticles

1. Introduction

Given the complexity of real heterogeneous catalysts [1] it is mandatory to simplify the problem in a way that an essential part of the complexity is included in a model system but it is still possible to apply methods that allow one to investigate the system at the atomic level [2–11]. A possible approach is to combine scanning probe microscopies with spectro-scopic and temperature programmed desorption techniques. Typically applied to single crystal surfaces under ultrahigh vacuum (UHV) conditions, model systems, based on thin well-ordered oxide films, can be studied with such techniques under the same but also ambient conditions. Nanoparticles of the desired chemical composition are then grown on top of such films in order to simulate the situation found in real catalytic samples where often small metal particles or oxide particles represent the active part of the catalyst.

Here we review results on deposited Pd nanoparticles in connection with hydrocarbon hydrogenation reactions [12–15] as well as vanadia particles grown on alumina and silica where we have been interested in understanding the growth and vibrational properties of the supported vanadia material which are interesting oxidation catalysts [16].

* Tel.: +49 30 84134102; fax: +49 30 84134101.
E-mail address: freund@fhi-berlin.mpg.de

0920-5861/$ – see front matter © 2005 Elsevier B.V. All rights reserved.
doi:10.1016/j.cattod.2004.12.021

2. Experimental

The experiments have been performed in a number of different ultrahigh vacuum apparatuses as well as reactor systems attached to those. Details on Pd particles on alumina can be found in [6], while experimental procedures and detail for the vanadia materials are reported in [16].

3. Results and discussion

We report and discuss first the individual results for the two systems under consideration and then generalize at the end with respect to the investigation of model systems per se.

Hydrogenation of unsaturated hydrocarbons occurs efficiently on noble-metal catalysts, such as platinum, rhodium, and palladium [17]. The reaction mechanism first proposed by Horiuti and Polanyi [18] in 1934 proceeds by: (a) hydrogen dissociation on the metal surface; (b) alkene adsorption; (c) subsequent hydrogen addition to alkene; and finally (d) desorption of the product (alkane). Real hydrogenation catalysts represent very complex systems for studying reaction mechanisms at the molecular level. Therefore, model systems have been invoked ranging from single crystals to metal particles deposited on oxide films [2–11].

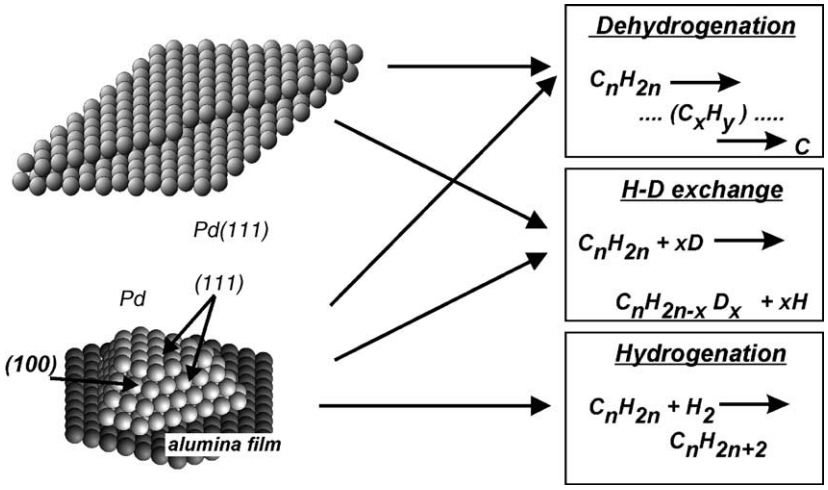

Fig. 1. Schematic representation of the alkene reactions observed on Pd(1 1 1) single crystal and well-faceted Pd particles supported on a thin alumina film.

We have studied the surface chemistry of ethene and different pentene isomers on both Pd(1 1 1) single crystal and Pd particles deposited on a thin alumina film (Fig. 1).

The particles studied are approximately 1–5 nm in diameter and consist primarily (∼90%) of (1 1 1) facets [6] (∼10% are (1 0 0) facets). The experiments were performed in ultrahigh vacuum on clean and well-defined systems. Using the temperature-programmed desorption (TPD) technique, we have observed that a number of hydrocarbon transformations, such as dehydrogenation and H-D exchange, occur on both palladium systems. However, the hydrogenation to alkane only occurs on small particles.

Adsorption of light alkenes, such as ethene, on palladium has been the subject of extensive studies on single-crystal surfaces and supported catalysts. [19,20] There is considerably less data on the interaction of higher hydrocarbons [21–24].

Madix and co-workers studied the adsorption of various alkenes and dienes on the clean and hydrogen (deuterium) precovered Pd(1 1 1) and Pd(1 0 0) surfaces by TPD [21,22]. They observed an H-D exchange reaction, which was assumed to proceed via a half-hydrogenated intermediate species. However, formation of the alkane was not observed on both surfaces.

We have examined the reactions of ethene, 1-pentene, *trans*- and *cis*-2-pentene on Pd(1 1 1) single crystals and supported Pd particles [25–27].

In the first part we review our own studies of hydrogenation of ethene in order to investigate the size-reactivity relationship on Pd nanoparticles. It is useful to recall and summarize the adsorption and dehydrogenation behavior of ethene without the presence of hydrogen.

Combining the results from thermal desorption spectroscopy (TDS) and IRAS [28–30], a general scheme for ethene thermal transformations on Pd particles has been proposed, as depicted schematically in Fig. 2. On small Pd particles, ethene is mainly π-bonded at low temperatures and desorbs intact upon heating. On the larger Pd particles, however, a fraction of the ethene molecules are di-s bonded. Again, weakly bonded ethene desorbs intact (its conversion to di-s species on heating cannot be excluded, however), while di-s ethene can either desorb near room temperature or dehydrogenate, producing surface species such as ethylidyne and atomic hydrogen. Dehydrogenation proceeds further on heating until a hydrogen-deficient carbonaceous deposit and hydrogen are formed at elevated temperatures. Hydrogen atoms recombine and desorb as hydrogen molecules. Finally, the surface remains covered by carbon deposits at elevated temperatures.

Accordingly, particle size and roughness strongly influence the distribution of π- and di-s-bonded ethene molecules. Due to the development of more extended facets on the large particles, which favor ethene di-s bonding, the reaction pathway shifts toward dehydrogenation and hence to the formation of carbon deposits upon heating.

For pure hydrogen adsorption two adsorption states can be distinguished. One state, leading to desorption around 330 K, is very likely due to hydrogen atoms on the surface of the particles, while a second one desorbing at lower temperatures (β1 at ∼280 K) is tentatively assigned to subsurface hydrogen [31,32]. As a function of particle size, β2 shifts to lower temperature with increasing particle size d, ranging from 1 nm $< d <$ 5 nm. The formation of the β1 state is decreased on the smallest particles, its desorption temperature being less influenced by the size of the particles. This can be a result of the decreasing number of subsurface sites available or due to the presence of the support.

Fig. 2 summarizes data for both ethane, pentene and hydrogen adsorption, as well as the corresponding hydrogenation reactions.

The top and bottom panel contain TDS data for ethane (bottom) and pentene (top) for a given average particle size, and the middle panel summarizes turn-over-numbers for hydrogenation of both pentene and ethane under ultrahigh vacuum conditions including a comparative study of ethene hydrogenation on the model system under ambient, higher

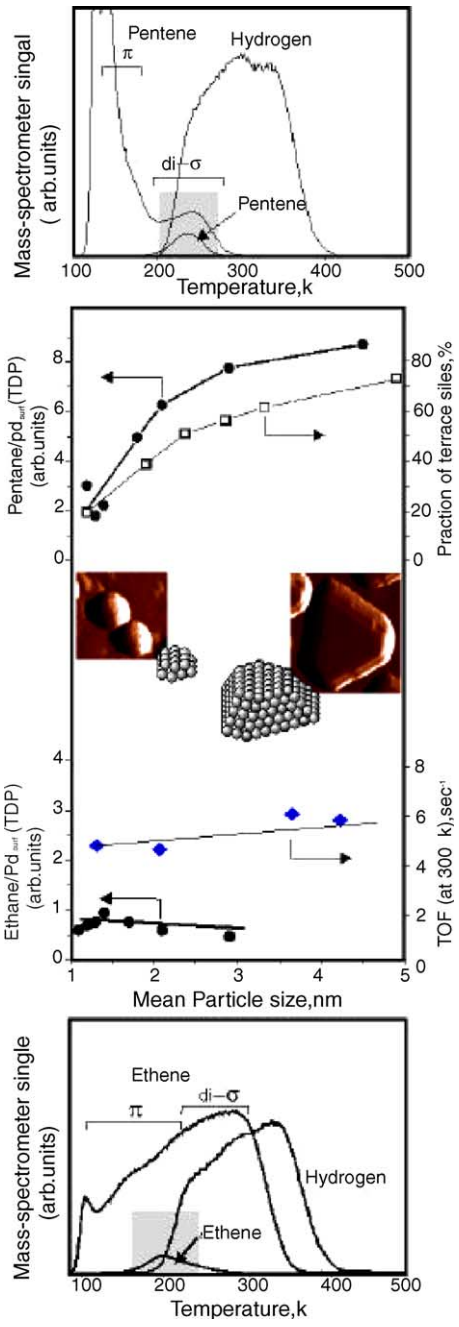

Fig. 2. (Middle panel): ethane and pentane production per Pd surface atom after ethen (lower two traces) and penten (upper trace) adsorption, respectively as a function of particle size. Together with the pentane data the fraction of terrace sizes as a function of particle size has been plotted. For ethane data taken under UHV conditions (filled circles) are compared with data taken in a batch reactor (diamonds) (conditions see text). (Upper and lower panel): temperature programmed desorption data for pentene (upper panel) and ethene (lower panel) desorption for the following particle sizes (3.2 nm for pentene and 1.7 nm for ethane) after Co-adsorption of hydrogen and the hydrocarbon.

pressure conditions. Starting the discussion with ethene we recorded TDS spectra of hydrogen, ethene and ethane. Comparing these spectra, first, we observe the formation of ethane, desorbing at −200 K as the product of ethene hydrogenation. Second, when hydrogen is present in the particles the amount of ethene desorbing at temperatures below 200 K is significantly increased, while the intensity of the state at about 280 K is reduced by a factor of 2. Therefore, the data indicate that it is the formation of di-s ethene that is inhibited by hydrogen adatoms. This can be understood by assuming that the surface hydrogen atoms, residing presumably in the hollow sites, sterically hinder the di-s bonding. Meanwhile, ethene can readily adsorb onto the hydrogen-covered surface via a π-bond on on-top sites. Therefore, hydrogen preadsorption leads to a redistribution of π- and di-s-bonded ethene, thus favoring a weakly bonded π-state.

In the reverse experiments, when the Pd particles were ethene precovered before exposure to hydrogen, the spectra were found to be identical to those when there was no hydrogen exposure at all. This manifests a site-blocking effect of ethene on hydrogen adsorption. Such an effect can be readily explained by the fact that hydrogen dissociation occurs on on-top sites (see review in [33], which are preferred by π-bonded ethene.

In the absence of preadsorbed hydrogen, a very small amount of ethane desorbing at ca. 280 K was detected only for particles larger than 30 Å. This process, called self-hydrogenation, involves the reaction of ethene with hydrogen adatoms produced by dehy-drogenation of other ethene molecules. Certainly, such a reaction occurs only on relatively large particles due to an increasing probability of ethene dehydrogenation. Nevertheless, the amount of ethane produced by self-hydrogenation is negligibly small as compared to that detected in coadsorption experiments. Moreover, the desorption temperature of ethane formed under coadsorption conditions is about 80 K lower than in a self-hydrogenation reaction (200 K versus 280 K). Such behavior (a temperature shift and an enhanced ethane production) has also been found on hydrogen-precovered Pt(1 1 1) [34] and Pd(1 1 0) [35] surfaces. Therefore, it appears that a general mechanism of ethene interaction with hydrogen on metal surfaces is valid on both single crystals and small metal particles. Our TDS study [28] shows that ethene reacts with the most weakly bonded hydrogen present on the surface. The formation of ethane depends on the presence of weakly adsorbed hydrogen, which reacts with π-bonded ethene before the latter desorbs intact.

The top panel shows results for pentene desorption from Pd particles after hydrogen pre-saturation superimposed with the hydrogen desorption data. A small amount of pentane desorbs within the temperature range of overlaps of the TDS traces. This is very similar to the case of ethene except that the peak in pentene TDS corresponds to the di-s-bonded molecule rather than the π-bonded species, which desorbs at lower temperature. Thus, the reaction starts from different precursors for the two hydrocarbons and it will be shown further below that this observation has major consequences for the particle size dependence of the reaction. Before we come to this issue it is interesting to

note that neither ethene nor pentene can be hydrogenated on Pd(1 1 1) single crystal under ultrahigh vacuum conditions. From comparison with literature data it is clear that the Pd particles contain a significant fraction of hydrogen more weakly bound then on Pd(1 1 1) surfaces, even though the Pd nanoparticles are mainly terminated by (1 1 1) facets. It is this weakly bound hydrogen that is involved in the reaction, and the difference in hydrogenation activity of Pd(1 1 1) as opposed to the nanoparticles seems too simply stem from the enhanced accessibility of the hydrogen atoms on the particles as a result of their nanoscale dimensions. This explains why nanopar-ticles are more active than single crystals for alkene hydrogenation on Pd under vacuum conditions. However, under real reaction conditions, it is likely that hydrogenation occurs on Pd crystals, owning to the enhanced accessibility of subsurface hydrogen formed at higher pressures.

In order to study particle size effects, we have carried out experiments for identical preparations varying only the amount of deposited Pd which leads to a change in average particle size as discussed in detail in the literature [6].

In the middle panel (lower trace) of Fig. 2 we plot ethane production per Pd unit surface area as a function of particle size. This plot clearly demonstrates that the hydrogenation activity under the coadsorption conditions studied, is almost independent of the Pd particle size in the range 1–3 nm. Such behavior can be understood by the fact that preadsorbed hydrogen strongly inhibits the formation of di-s-bonded ethene and results in preferential formation of the π-bonded ethene for all particle sizes studied, thus neutralizing the overall particle size influence. The size independence for ethene hydrogenation obtained in the present work agrees well with the general opinion that this reaction is structure-insensitive [36], and it seems that our system represents a suitable model system for studying the mechanism of the reaction, even using UHV conditions. Fig. 2 shows turnover frequencies as a function of particle size measured on model catalysts prepared in the same way as used for the ultra-high-vacuum studies (middle panel (diamonds)) [26,37,38]. The model catalyst was placed in a reaction vessel [39] and exposed to a mixture of C_2H_4 (50 mbar), H_2 (215 mbar), and He (770 mbar), with ethane production being monitored by on-line gas chromatography at various temperatures and reaction times [37]. Knowing the structure and morphology of the catalyst, turnover frequencies are calculated. The system turned out to be stable under reaction. The TOFs are rather independent of particle size and the activation energy for ethene hydrogenation from temperature-dependent data is ca. 55 kJ/mol [37]. There is a remarkable correspondence of particle-size-dependent properties under ultrahigh vacuum and ambient conditions, which already at this stage can be taken as indication that the mechanisms are similar under both conditions.

If we now investigate particle size effects for pentene hydrogenation we find the result shown in the middle panel Fig. 2 (upper trace). There is a clear particle size dependence indicating considerable structure sensitivity in this case as opposed to ethene hydrogenation. This rather surprising result can be well understood on the basis of the different hydrogenation precursors for ethene and pentene. While for ethene it is the π-bonded species that turns over, it is the di-s-bonded species for pentene. The abundance of the di-s-bonded species increases with increasing particle size as the particles expose more well-ordered facets when they grow. This is reflected by the observed increase of turn-over by about a factor of 4. This increase in hydrogenation activity correlates well with the ratio of terrace sites to total surface Pd atoms shown on the same diagram. The correlation strongly indicates that the terrace sites favor *trans*-2-pentene hydrogenation. This result also supports the conclusion that pentene hydrogenation proceeds via the di-s-bonded species as the precursor. Indeed, adsorption in a di-s-bonded geometry occurs preferentially on flat surfaces, which are characteristic for the larger particles [25]. As a result, the activity increases with particle size, indicating that *trans*-2-pentene hydrogenation is structure sensitive.

This difference in the size dependence observed for ethene and pentene is considerable, even though the di-s state is more favorable on terraces for both molecules, and therefore, one would expect similar behavior for both alkenes. However, Neurock and van Santen [40] using cluster and DFT calculations, showed that it is π-bonded ethene, rather than di-s-bonded ethene, that converts to an ethyl group (and subsequently to ethane), when adsorbed at high coverage on the H-precovered Pd(1 1 1) surface. This is consistent with our experimental data showing that π-bonded ethene is the active species in ethene hydrogenation [15,19,36,41] and may explain the structure insensitivity of ethene hydrogenation. To our knowledge, there are no similar calculations for pentene. However, it is expected that hydrocarbons, beginning with propene, adsorb in a less distorted geometry (π-bonded) in a second layer [42,43], i.e. on top of the most strongly bound di-s species. In other words, π-bonded species may not be in direct contact with the Pd surface. Therefore, it seems plausible that π-bonded pentene on the H(D) pre-covered Pd surface desorbs intact, and the hydrogenation proceeds only via di-s bonded pentene, in contrast to π- and di-s-bonded ethene, which transform into ethyl intermediates.

The second part of this review contains a short summary of work concerning the characterization of supported vanadia model systems with respect to vibrational properties.

Fig. 3 shows STM images of intermediate VO_x particle coverages on SiO_2 and Al_2O_3. Typical particle diameters are in the range of 2–3 nm, but owing to STM tip convolution effects, these values are generally overestimated by up to a factor of 2. The particles are characterized by XPS as vanadiumsesquioxide (V_2O_3) particles in the volume. On its surface they carry, however, vanadyl (V=O) groups as will become clear when we discuss vibrational spectra further

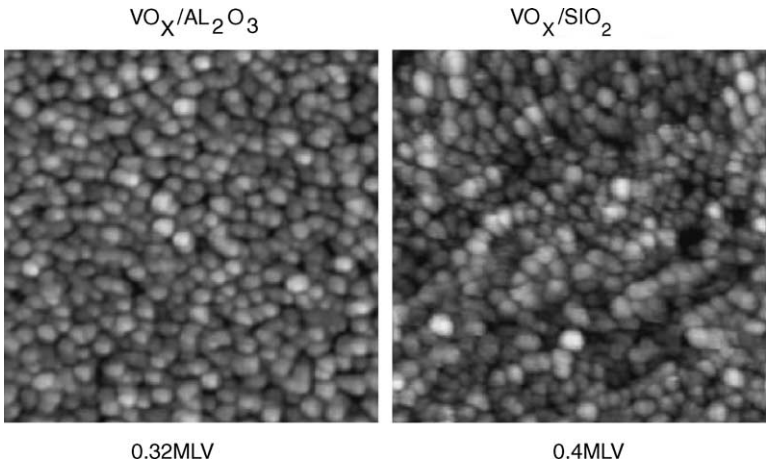

Fig. 3. Comparison of two STM images (50 nm × 50 nm) measured for alumina- and silica-supported vanadia particles of similar V-content. Tunneling was performed at the following conditions: $U = 2.2$ V, $I = 0.07$ nA (VO_x/Al_2O_3); $U = 3.3$ V, $I = 0.12$ nA (VO_x/SiO_2). In both cases, particle number densities between $\sim 1.8 \times 10^{13}$ and 1.9×10^{13} particles per cm^{-2} were determined.

below. This is in full accord with investigations on $V_2O_3(0\,0\,0\,1)$ surfaces where it has been shown that the surface is vanadyl-terminated. The latter implies that the surface vanadium-oxide ions are in a higher oxidation state (+5) as also experimentally revealed through angle dependent XPS measurements again carried out on $V_2O_3(0\,0\,0\,1)$ thin film surfaces [44]. Fig. 4 presents a series of IR spectra measured as a function of vanadia loading in alumina and silica supports [45].

The starting-point is a clean alumina film, which is characterized by several sharp phonon bands, the most prominent of which is located at 866 cm^{-1}(left panel, Fig. 4). Upon increasing V-exposure, this feature attenuates very rapidly, indicating a strong interaction between vanadia and alumina. Concomitantly, two new signals appear at higher vibrational energies whose intensities saturate after ~1 ML V. For multilayers, a third signal was detected at ~700 cm^{-1}, which can be assigned to vibrations of a V–O–V bulk-species. A similar feature has been observed on thick V_2O_3-films grown on Pd(1 1 1) [46]. In contrast, the two other vibrations have to be localized either at the surface of the vanadia particles or at their interface to the alumina support. Comparison with literature data revealed that the highest frequency band which shifts from ~1025 cm^{-1} to ~1045 cm^{-1} with increasing V-exposure, is due to terminating vanadyl groups (V=O) [47,48]. The band at ~941 cm^{-1} involves vibrations of Al, O and V ions (Al–O–V) [49]. This vibration is restricted to the interface region and is a result of strong vanadia–alumina interactions. CO experiments performed on this system provided further evidence for these assignments [50,51].

IR spectra for VO_x/SiO_2 are shown in Fig. 4 (right panel, Fig. 4). The clean silica film is dominated by a narrow phonon band at 1048 cm^{-1} with a shoulder at lower energy.

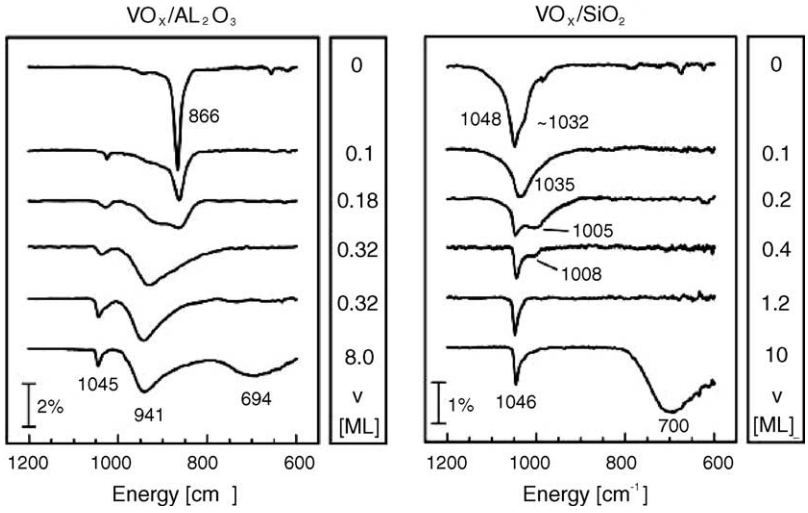

Fig. 4. IR spectra from alumina- and silica-supported vanadia particles as a function of V-coverage. All spectra were measured at 300 K and referenced to the underlying NiAl and Mo metal substrates, respectively.

Upon vanadium deposition, these Si–O vibrations attenuate and broaden, while their frequency shifts to ~1035 cm^{-1}, and finally to ~1005–1008 cm^{-1} (note that these shifts are quite large as compared to phonon shifts observed on alumina [52] but are similar to those found for UHV-deposited vanadium on silica [50,51]). After 0.4 ML V, the Si–O band has nearly disappeared. The same is true for the characteristic silica LEED pattern, which has become very faint with a high background intensity. Simultaneously, a new species has appeared at ~1046 cm^{-1} whose properties – peak position and width, interaction with adsorbed CO [50,51] – correspond to those of the V=O groups on VO_x/Al_2O_3. At very high coverages, a V–O–V bulk-species is observed in the same frequency regime as on alumina thus underlining the similarity between the two systems.

Note, however, that the situation is more complicated in the case of VO_x/SiO_2 than it seems on first sight. This is due to the proximity of V=O and Si–O vibrations, which might couple with each other. In addition, DFT calculations on model components predict intense Si–O–V vibrations with frequencies in the range of ~1000–1030 cm^{-1} (Fig. 3). These in-phase symmetric stretching vibrations should be visible in our IR spectra and one might suspect that the signal detected at ~1005 cm^{-1} represents species of that kind instead of attenuated Si–O vibrations. However, its intensity development is completely different from that of the Al–O–V mode. While the band on silica vanishes at intermediate V-coverages, the Al–O–V band grows until an exposure of ~1 ML V and remains constant thereafter [45].

In conclusion, we can neither prove nor exclude the presence of Si–O–V interface modes in our IR spectra on the basis of the experiments so far. Nevertheless, it is clear that the interaction between vanadium and the oxide support is considerably weaker for VO_x/SiO_2 than for VO_x/Al_2O_3. This is corroborated by experiments where isolated vanadium carbonyls were generated on both oxide films. On alumina, this was possible at a temperature of 300 K, while for silica the sample had to be cooled to 90 K in order to reduce the diffusion length of deposited V-atoms to such an extent that a sufficient number of single atoms was formed [50,51,53]. The findings on the model systems are in accord with Raman data on powder samples. It turns out that it is possible to find a unique interpretation of spectra of model systems and powder samples based on the analysis of theoretical calculations. However, the findings are not completely consistent with the view generally discussed in the literature and we propose that this view has to be revised.

In particular, the so-called vanadyl vibrations cannot, in general, be assumed to be independent of the substrate and thus cannot be used as an indicator for monomeric and polymeric species. In fact, it is much more the coupling of the vanadia to the support that has to be considered in the interpretation of the spectra. By using two different supports, namely silica and alumina, we prove the dominance of interface vibrations in both infrared and Raman spectra based on the results of cluster calculations in conjunction with morphological studies using the STM.

It is this combination of experimental techniques and calculations that allows us to draw conclusions on the correlation of structure and spectroscopy which otherwise are difficult or even impossible to reach.

4. Summary

The present two examples of model studies in heterogeneous catalysis are chosen to underline the usefulness of such studies. The first example on hydrogenation on Pd nanoparticles demonstrates the necessity to study systems of sufficient complexity to be able to catch some of the characteristics of the ''real'' system, however, kept at the same time sufficiently simple to be able to study the system with surface science tools. Very clearly we show that single crystal surfaces are too simple a system due to the existence of a basically ''infinitely'' large volume. The finite size and morphology of the nanoparticles promote hydrogen diffusion into the subsurface area. It is the fact that this hydrogen cannot ''escape'' from the surface through bulk diffusion that determines the ease of hydrogenation reactions on Pd catalysts. At the same time it is the morphology of the particle surface that determines the mechanism and the particle size dependence of the reaction. In fact, the general notion that hydrogenation reactions are structure in-sensitive because there is no particle size dependence is shown to be an overstatement. As soon as s-bonded unsaturated hydrocarbons are involved as intermediates, as it is shown for the case of *trans*-2-pentene, the reaction preferentially proceeds on well-ordered facets, which are more frequently observed for the larger nanoparticles. Thus the reactions become structure sensitive. It is noted that the turn-over-numbers observed under vacuum conditions favorably compare with those measured on the same model catalyst under ambient conditions with a gas chromotograph.

The second example is meant to demonstrate that model systems may be crucial to pin down structure/morphology–spectroscopy relations, which are in the case of supported oxide systems often used to infer structure-reactivity relations. The morphology of so-called ''monolayer'' vanadia catalysts on alumina and silica are imaged to contain a dense arrangement of nanoparticles. It is possible on these model systems to carry out vibrational spectroscopy and in street comparison with quantum theoretical calculations to assign those spectra in a unique way. The study demonstrates that a clear distinction between vibrations involving constituents of the nanoparticles only and those involving the nanoparticles-support interface is possible. The study also indicates the necessity to revisit some of the accepted interpretations of vibrational spectra of supported oxides.

I believe that the study of model systems has a future that allows us to merge catalysis with surface science and that this development will be fruitful for both fields.

Acknowledgments

I am grateful to DFG (SFB 546 ''Struktur, Dynamik und Reaktivität von Über-gangsmetalloxid-Aggregate'', SPP 1091 ''Brückenschläge zwischen idealen und realen Systemen in der heterogenen Katalyse''), ATHENA Project funded by EPSRC and Johnson Matthey, COMBICAT Malaysia and Fonds der Chemischen Industrie for support. I acknowledge with gratitude the contribution of my collaborators whose names appear in the references.

References

[1] G. Ertl, H. Knözinger, J. Weitkamp (Eds.), Handbook of Heterogeneous Catalysis, vol. 4, Wiley-VCH Verlagsgesellschaft mbH, Weinheim, 1997, p. 1560.
[2] H.-J. Freund, Ber. Bunsenges. Phys. Chem. 99 (1995) 1261.
[3] H.-J. Freund, Angew. Chem. Int. Ed. Engl. 36 (1997) 452.
[4] M. Bäumer, J. Libuda, H.-J. Freund, in: R.M. Lambert, G. Pacchioni (Eds.), Chemisorption and Reactivity on Supported Clusters and Thin Films, vol. 331, Kluwer, Dordrecht, 1997, p. 61.
[5] G. Ertl, H.-J. Freund, Phys. Today 52 (1999) 32.
[6] M. Bäumer, H.-J. Freund, Prog. Surf. Sci. 61 (1999) 127.
[7] H.-J. Freund, Surf. Sci. 500 (2002) 271.
[8] H.-J. Freund, J. Libuda, M. Bäumer, T. Risse, A.F. Carlsson, Chem. Rec. 3 (2003) 181.
[9] D.W. Goodman, Surf. Rev. Lett. 2 (1995) 9.
[10] C.T. Campbell, Surf. Sci. Rep. 27 (1997) 1.
[11] C.R. Henry, Surf. Sci. Rep. 31 (1998) 231.
[12] A.M. Doyle, S. Shaikhutdinov, H.-J. Freund, Angew. Chem. 44 (2005) 624.
[13] A.M. Doyle, S. Shaikhutdinov, H.-J. Freund, Angew. Chem., in press.
[14] A.M. Doyle, S. Shaikhutdinov, H.-J. Freund, J. Catal. 223 (2004) 444.
[15] H.-J. Freund, M. Bäumer, J. Libuda, T. Risse, G. Rupprechter, S. Shaikhutdinov, J. Catal. 216 (2003) 223.
[16] N. Magg, B. Immaraporn, J. Giorgi, T. Schroeder, M. Bäumer, J. Döbler, Z. Wu, E. Kondratenko, M. Cherian, M. Baerns, P.C. Stair, J. Sauer, H.-J. Freund, J. Catal. 226 (2004) 88.
[17] G. Webb, Compr. Chem. Kinet. 20 (1978) 1.
[18] J. Horiuti, M. Polanyi, Trans. Faraday Soc. 30 (1934) 1164.
[19] N. Sheppard, C.D.L. Cruz, Adv. Catal. 41 (1996) 1.
[20] N. Sheppard, C.D.L. Cruz, Adv. Catal. 42 (1998) 181.
[21] X.-C. Guo, R.J. Madix, J. Catal. 155 (1995) 336.
[22] N.J. Vasquez, R.J. Madix, J. Catal. 178 (1998) 234.
[23] J.C. Bertolini, A. Cassuto, Y. Jugnet, J. Massardier, B. Tardy, G. Tourillon, Surf. Sci. 349 (1996) 88.
[24] N.A. Thornburg, I.M. Abdelrehim, D.P. Land, J. Phys. Chem. B 103 (1999) 8894.
[25] S. Shaikhutdinov, M. Heemeier, M. Baumer, T. Lear, D. Lennon, R.J. Oldman, S.D. Jackson, H.-J. Freund, J. Catal. 200 (2001) 330.
[26] S. Shaikhutdinov, M. Frank, M. Bäumer, S.D. Jackson, R.J. Oldman, J.C. Hemminger, H.-J. Freund, Catal. Lett. 80 (2002) 125.
[27] A.M. Doyle, S. Shaikhutdinov, H.-J. Freund, unpublished results.
[28] S.K. Shaikhutdinov, M. Heemeier, M. Bäumer, T. Lear, D. Lennon, R.J. Oldman, S.D. Jackson, H.-J. Freund, J. Catal. 200 (2001) 330.
[29] M. Frank, M. Bäumer, Phys. Chem. Chem. Phys. 2 (2000) 3723.
[30] M. Frank, M. Bäumer, R. Kühnemuth, H.-J. Freund, J. Vac. Sci. Technol. A19 (2001) 1497.
[31] H. Okuyama, W. Siga, N. Takagi, M. Nishijima, T. Aruga, Surf. Sci. 401 (1998) 344.
[32] D. Farias, M. Patting, K.H. Rieder, Phys. Stat. Sol. 159 (1997) 255.
[33] K. Christmann, Z. in, P.G. Paal, Menon (Eds.), Hydrogen Effects in Catalysis, Dekker, New York, 1988, p. 3.
[34] D. Godbey, F. Zaera, R. Yeates, G.A. Somorjai, Surf. Sci. 167 (1986) 150.
[35] T. Sekitani, T. Takaoka, M. Fujisawa, M. Nishijima, J. Phys. Chem. 96 (1992) 8462.
[36] G.A. Somorjai, Introduction to Surface Chemistry and Catalysis, Wiley, New York, 1994.
[37] G. Rupprechter, H. Unterhalt, M. Morkel, P. Galletto, L. Hu, H.-J. Freund, Surf. Sci. 502/503 (2002) 109.
[38] G. Rupprechter, H. Unterhalt, L. Hu, H.-J. Freund, J. Catal., in preparation.
[39] G. Rupprechter, T. Dellwig, H. Unterhalt, H.-J. Freund, Top. Catal. 15 (2001) 19.
[40] M. Neurock, R.A. van Santen, J. Phys. Chem. B 104 (2000) 11127.
[41] P.S. Cremer, G.A. Somorjai, J. Chem. Soc., Faraday Trans. 91 (1995) 3671.
[42] D. Stacchiola, L. Burkholder, W.T. Tysoe, Surf. Sci. 542 (2003) 129.
[43] F. Zaera, D. Chrysostomou, Surf. Sci. 457 (2000) 89.
[44] A.-C. Dupuis, M. Abu Al-Haija, B. Richter, H. Kuhlenbeck, H.-J. Freund, Surf. Sci. 539 (2003) 99.
[45] N. Magg, J.B. Giorgi, T. Schroeder, M. Bäumer, H.-J. Freund, J. Phys. Chem. B 106 (2002) 8756.
[46] M. Sock, S. Surnev, M.G. Ramsey, F.P. Netzer, Top. Catal 94 (2001) 4240.
[47] I.E. Wachs, Catal. Today 27 (1996) 437.
[48] G.T. Went, S.T. Oyama, A.T. Bell, J. Phys. Chem. 94 (1990) 4240.
[49] H. Miyata, K. Fujii, T. Ono, Y. Kubokawa, T. Ohno, F. Hatayama, J. Chem. Soc., Faraday Trans. 1 (83) (1987) 675.
[50] N. Magg, J.B. Giorgi, A. Hammoudeh, T. Schroeder, M. Bäumer, H.-J. Freund, J. Phys. Chem. B 107 (2003) 9003.
[51] N. Magg, Thesis, Humboldt Universität, 2003.
[52] M. Frank, K. Wolter, N. Magg, M. Heemeier, R. Kühnemuth, M. Bäumer, H.-J. Freund, Surf. Sci. Lett. 492 (2001) 270.
[53] N. Magg, J.B. Giorgi, M.M. Frank, B. Immaraporn, T. Schroeder, M. Bäumer, H.-J. Freund, J. Am. Chem. Soc. (2003).